Elsevier Editorial System(tm) for Journal of Colloid and Interface Science
Manuscript Draft

Manuscript Number: JCIS-14-2753R1

Title: Influence of the metal precursor on the catalytic behavior of Pt/CeO2 catalysts in the preferential oxidation of CO in the presence of H2 (PROX)

Article Type: Regular Article

Section/Category: C. Adsorption, Catalysis and Electrochemistry

Keywords: Metal precursor, Pt, ceria, PROX, DRIFTS

Corresponding Author: Prof. Antonio Sepúlveda-Escribano, PhD

Corresponding Author's Institution: University of Alicante

First Author: E.O. Jardim

Order of Authors: E.O. Jardim; Soledad Rico-Francés; Fernando Coloma-Pascual; James A Anderson; Joaquín Silvestre-Albero; Antonio Sepúlveda-Escribano, PhD

Abstract: The effect of the metal precursor (presence or absence of chlorine) on the preferential oxidation of CO in the presence of H2 over Pt/CeO2 catalysts has been studied. The catalysts were prepared using (Pt(NH3)4)(NO3)2 and H2PtCl6, as precursors, in order to ascertain the effect of the chlorine species on the chemical properties of the support and on the catalytic behavior of these systems in the PROX reaction. The results show that chloride species exert an important effect on the redox properties of the oxide support due to surface chlorination. Consequently, the chlorinated catalyst exhibits a poorer catalytic activity at low temperatures compared with the chlorine-free catalyst, and this is accompanied by a higher selectivity to CO2 even at high reaction temperatures. It is proposed that the CO oxidation mechanism follows different pathways on each catalyst.

3: Graphical Abstract (for review)

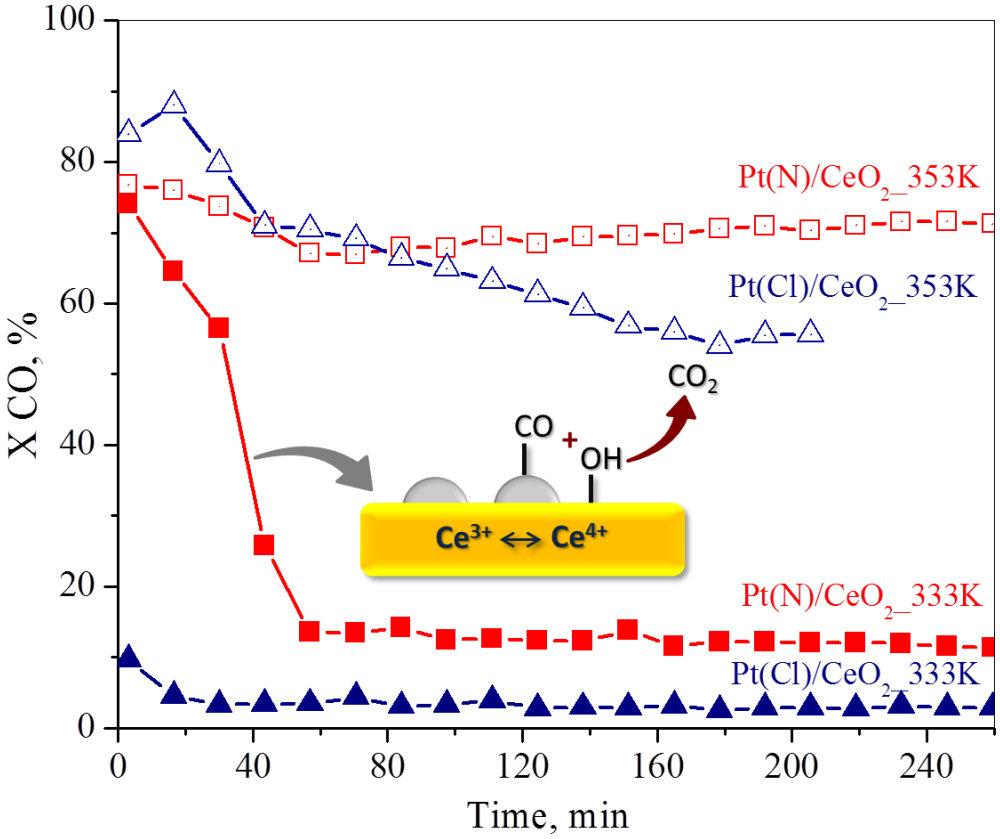

- The presence or absence of Cl in the Pt precursor strongly affects the catalytic behavior.
- The Pt precursor affects the PROX mechanism at low reaction temperatures.
- At 333 K, the mechanism in the Cl-free catalyst seems to involve the -OH groups on the support.
- At higher temperatures, the reaction occurs *via* the same mechanism on both catalysts.

.

Influence of the metal precursor on the catalytic behavior of Pt/CeO_2 catalysts in the preferential oxidation of CO in the presence of H_2 (PROX)

Erika O. Jardim[1], Soledad Rico-Francés[1], Fernando Coloma[1], James A. Anderson [2], Joaquín Silvestre-Albero[1] and Antonio Sepúlveda-Escribano[1].*

[1]Laboratorio de Materiales Avanzados, Departamento de Química Inorgánica – Instituto Universitario de Materiales de Alicante. Universidad de Alicante. Apartado 99, E-03080 Alicante, Spain.

[2]Surface Chemistry and Catalysis Group, Department of Chemistry and School of Engineering, University of Aberdeen, AB24 3UE Scotland (UK).

**Corresponding author:*
E-mail: asepul@ua.es
Tel: + 34 965903974
Fax: + 34 965903454

Abstract

The effect of the metal precursor (presence or absence of chlorine) on the preferential oxidation of CO in the presence of H_2 over Pt/CeO_2 catalysts has been studied. The catalysts are prepared using $(Pt(NH_3)_4)(NO_3)_2$ and H_2PtCl_6, as precursors, in order to ascertain the effect of the chlorine species on the chemical properties of the support and on the catalytic behavior of these systems in the PROX reaction. The results show that chloride species exert an important effect on the redox properties of the oxide support due to surface chlorination. Consequently, the chlorinated catalyst exhibits a poorer catalytic activity at low temperatures compared with the chlorine-free catalyst, and this is accompanied by a higher selectivity to CO_2 even at high reaction temperatures. It is proposed that the CO oxidation mechanism follows different pathways on each catalyst.

Keywords: Metal precursor, Pt, ceria, PROX, DRIFTS.

1. Introduction.

Hydrogen is a promising energy vector to be used to replace or complement the current energy model based on fossil fuels [1]. It is non-polluting if it is obtained from renewable sources, and can be easily and efficiently transformed into energy both chemically and electrochemically [2-5]. In this sense, the most promising technologies to obtain energy are based on fuel cells, with the proton exchange membrane fuel cell (PEMFC) standing out. Hydrogen can be obtained from a great variety of sources, including water, fossil fuels and biomass, and by different methodologies. Currently, the most widely used one is the steam reforming of methane, although many other hydrogen-containing compounds can be steam reformed. One of the main drawbacks of this process is the formation of CO as a by-product, as CO is a strong poison of PEMFC´s electrodes [1,6-9]. High concentrations of CO can be removed from the reformate streams by the water-gas shift reaction (WGS), during which it reacts with water to yield CO_2 and H_2. However, the residual concentration of CO is still usually too high to feed the PEMFCs and other fuel cells working at low temperatures.

The preferential CO oxidation (PROX) arises as a good alternative to reduce the amount of CO remaining after the WGS reaction to achieve tolerable values for the fuel cell (below10 ppm) [1]. Different catalysts have been studied in this reaction, with a great variety of supports and metals. The important role played by reducible oxides such as ceria has been shown, as they can participate in the reaction through activation of the water molecule [8].

The characteristics of the support can influence the reaction mechanism. Several mechanisms have been proposed in the literature for the PROX reaction, which may depend on the choice of catalyst support. Mariño *et al.* [10,11] have shown that the CO oxidation mechanism over non-active supports occurs *via* a competitive Langmuir-Hinshelwood mechanism, where CO and O_2 are adsorbed on the same adsorption sites. However, when a reducible metal oxide is used as a support, the oxygen anion functionalities of the support participate in the reaction, *via* a Mars-Krevelen mechanism [10-12]. Pozdnyakova *et al.* [13] suggested that the reaction mechanism in Pt/CeO_2 catalysts involves -OH groups on the surface. Their presence seems to suppress hydrogen oxidation while CO oxidation still takes place, as the metallic particles are covered by CO. This behavior minimizes the possibility of a direct reaction between adsorbed CO and O_2. Quinet *et al*. [14] suggested that the reaction mechanism over Au/Al_2O_3 catalysts involves the -H, -OH and -OOH intermediates adsorbed on gold

particles, and the bicarbonates, carboxylates and hydroxycarbonyls adsorbed either on the metal nanoparticles or on the metal-support interface. Daté *et al.* [15] and Debeila *et al.* [16] showed the effect of humidity in the reaction mixture for the CO oxidation at low temperature on Au/TiO_2, Au/Al_2O_3 and Au/SiO_2 catalysts. In this case, the presence of H_2O or –OH influences the reaction rate.

In this work, the catalytic behavior of Pt/CeO_2 catalysts in the CO oxidation reaction in the presence of H_2 has been studied. More specifically, the work deals with the effect of the nature of the metal precursor by comparing catalysts prepared with a Cl-containing and a Cl–free precursor. Besides the support characteristics, it is well known that the nature of the metal precursor used is important because it can yield chemical and structural differences. Furthermore, catalysts prepared from chlorine-containing precursors are liable to incorporate a large amount of chloride ions into the support [16]. Kepinski *et al.* [17] studied the mechanism of CeOCl formation in Pd/CeO_2 catalysts prepared using a chlorinated precursor, $PdCl_2$. These authors suggested that at low reduction temperatures, Cl^- ions remain strongly chemisorbed on ceria. However, an increase in the reduction temperature produces a progressive incorporation of the chloride ions into the oxygen vacancies of the support. From HRTEM studies, it was possible to identify CeOCl species after reduction at temperatures between 423 and 573 K. An increase in the reduction temperature up to 673 K led to growth of these CeOCl crystallites, as confirmed by XRD. Moreover, in addition to the growth of the CeOCl crystals, an important loss of the catalyst surface area was observed. This fact indicates that the incorporation of the chloride ions induces changes in the textural, structural and chemical properties of the support. Thus, it can be concluded that both the support characteristics and the metal precursor used will have a large influence on the CO oxidation reaction mechanism.

With this in mind, we have studied in this work the effect of the metal precursor in the CO oxidation reaction on Pt/CeO_2 catalysts. Catalysts have been deeply characterized and the catalytic activity has been monitored by gas chromatography and by diffuse reflectance infrared Fourier transform spectroscopy (DRIFTS) analysis with online mass spectrometry.

2. Experimental.

2.1. Preparation of the Pt catalysts.

The cerium oxide support was prepared by homogeneous precipitation. 13 g of $Ce(NO_3)_3 \cdot 9H_2O$ (Aldrich, 99%) and 8 g of urea (Fluka, 98%) were dissolved in 400 ml of ultra-pure water. The mixture was heated at 363 K with constant stirring for 11 h. Finally, ammonia solution was added drop-wise to ensure complete precipitation. The solid was separated by filtration, washed with ultra-pure water and finally dried at 383 K overnight. The powder sample was calcined at 773 K for 4 h, reaching this temperature at a heating rate of 3 $K \cdot min^{-1}$. Two different Pt/CeO_2 catalysts were prepared by the wetness impregnation method, using different precursors. The support was impregnated with aqueous solutions of $(Pt(NH_3)_4)(NO_3)_2$ (Aldrich, 99.9%) (catalyst $Pt(N)/CeO_2$) or H_2PtCl_6 (Alfa Aesar, 99.9%) (catalyst $Pt(Cl)/CeO_2$) with the appropriate concentrations to achieve a 1 wt.% Pt loading. Finally, the catalysts were dried at 383 K overnight and calcined at 773 K for 2 h, after heating to this temperature at 3 $K \cdot min^{-1}$.

2.2. Catalysts characterization.

The textural properties of the supports were characterized by nitrogen adsorption measurements at 77 K. Gas adsorption experiments were performed in a home-made fully automated manometric apparatus. Prior to the adsorption experiments, samples were out-gassed under vacuum (10^{-4} Pa) at 523 K for 4 h. The BET surface area was estimated after application of the BET equation.

The actual metal loading of the different catalysts was determined by ICP in a Perkin–Elmer device (Optimal 3000). To this end, the metal was extracted from the catalysts by refluxing them in aqua regia for 8 h.

X-Ray powder diffraction patterns were recorded on a Bruker D8-Advance with a Göebel mirror and a Kristalloflex K 760-80 F X-Ray generation system, fitted with a Cu cathode and a Ni filter. Spectra were registered between 20 and 80º (2θ) with a step of 0.05º and a time per step of 3s.

TEM observations were carried out on a JEOL electron microscope (model JEM-2010) working at 200 kV. It was equipped with an INCA Energy TEM 100 analytical system and a SIS MegaView II camera. Samples for analysis were suspended in ethanol and placed on copper grids with a holey-carbon film support.

Temperature-programmed reduction (TPR) with H_2 measurements were carried out on calcined catalysts in a U-shaped quartz cell using a 5% H_2/He gas flow of 50 $ml \cdot min^{-1}$, with a heating rate of 10 $K \cdot min^{-1}$. Samples were treated with flowing He at 423 K for 1 h before the TPR run. Hydrogen consumption was followed by on-line

mass spectrometry and calibrated by carrying out the reduction of CuO and assuming complete reduction to metallic copper.

X-Ray photoelectron spectroscopy was performed with a VG-Microtech Multilab 3000 spectrometer equipped with a hemispherical electron analyzer and a Mg-K_α (h=1253.6 eV; 1 eV = 1.6302×10^{-19} J) 300-W X-ray source. The powder samples were pressed into small Inox cylinders, mounted on a sample rod placed in a pretreatment chamber, and reduced in flowing H_2 for 1 h at 523 and 773 K before being transferred to the analysis chamber. Before recording the spectrum, the sample was maintained in the analysis chamber until a residual pressure of *ca.* 5×10^{-7} N·m^{-2} was reached. The spectra were collected at pass energy of 50 eV. The intensities were estimated by calculating the integral of each peak, after subtracting the S-shaped background, and by fitting the experimental curve to a combination of Lorentzian (30%) and Gaussian (70%) lines. All binding energies were referenced to the C 1s line at 284.6 eV, which provided binding energy values with an accuracy of ± 0.2 eV. The surface Cl/Ce atomic ratios were estimated from the integrated intensities corrected using the atomic sensitivity factors [18].

Temperature-programmed desorption of CO (CO-TPD) from the support and from the calcined catalysts was carried out in a U-shaped quartz cell using a 10% CO in He with a gas flow of 50 ml·min^{-1}. Samples were reduced with flowing H_2 at 523 K (5 K·min^{-1}) for 1 h and then cooled to room temperature in He flow at 50 ml·min^{-1} before CO adsorption, which was carried out by exposing the sample to a 10% CO/He flow for 1 h. Physisorbed CO was removed by purging with He. CO/CO_2 desorption was performed under a He flow until 773 K, with a heating rate of 10 K·min^{-1} and followed by on-line mass spectrometry.

2.3. Catalytic behavior.

For the determination of the catalytic behavior, the catalysts were placed in a U-shaped quartz reactor. Before any catalytic measurement, the catalysts were reduced *in-situ* under flowing hydrogen (50 ml·min^{-1}) at 523 or 773 K for 1 h (heating rate of 5 K·min^{-1}). The PROX reaction was studied in the temperature range 313 - 473 K and at atmospheric pressure. The reaction mixture contained 20% H_2, 2% CO, 0.6-2% O_2 and He as balance (total flow: 50 ml·min^{-1} and GHSV (Gas hourly space velocity) = 17000 h^{-1}). Reaction products were analyzed by online gas chromatography (TCD and FID),

using a Plot/Q and a Molesieve capillary column to separate the reactants and the reaction products. Only CO_2 and H_2O were detected as products.

Diffuse reflectance infrared Fourier transform spectroscopy (DRIFTS) analysis was used to evaluate the adsorbed species present on the catalyst under reaction conditions. DRIFT spectra were collected using a Perkin-Elmer 100 FTIR fitted with an MCT detector. On-line gas analysis was performed using a Baltzers Prisma Quadrupole mass spectrometer. The DRIFTS cell (Harrick DRP-series) was fitted with ZnSe windows. Before exposure to the reactant gas mixture, samples were reduced *in situ* under flowing hydrogen (40 ml/min) at 523 K for 1 h, at a heating rate of 5 K/min. DRIFT spectra were recorded at 4 cm^{-1} resolution as an average of 10 scans. The gas mixtures were prepared using a computer-controlled gas-blender (Signal) with 40 ml/min passing through the catalyst bed which equates to a GHSV of 17000 h^{-1} using about 100 mg of sample. CO oxidation was studied between 313 and 473 K, with a reactant mixture containing 20% H_2, 2% CO, 10% air and N_2 as a balance.

The CO conversion (X_{CO}), O_2 conversion (X_{O2}) and the selectivity (S) towards CO_2, as well as the yield to CO_2 and the λ value, were calculated using the following equations [8]:

$$X_{CO} = 100 \cdot ((CO)_{in} - (CO)_{out})/(CO)_{in}$$

$$X_{O2} = 100 \cdot ((O_2)_{in} - (O_2)_{out})/(O_2)_{in}$$

$$S = 100 \cdot 0.5 \cdot ((CO)_{in} - (CO)_{out})/((O_2)_{in} - (O_2)_{out})$$

$$Yield = X_{CO}/100 \cdot S_{CO2}/100$$

$$\lambda = 2 \cdot (O_2)/(CO)$$

3. Results and discussion.

3.1. Catalyst characterization.

The BET surface area of the different materials used, as well as the platinum and chlorine content for chlorine-free and chlorine-containing catalysts as determined by ICP are reported in Table 1. The CeO_2 support, prepared by homogeneous precipitation

with urea, exhibited a very high surface area of 110 $m^2 \cdot g^{-1}$, as compared with the same material prepared by other conventional methods (e.g. precipitation with ammonium carbonate (S_{BET}: 70 $m^2 \cdot g^{-1}$)) [19]. Metal addition, including post-calcination produced a decrease of the BET surface area. Furthermore, some chlorine remained in the Pt(Cl)/CeO_2 catalyst, even after calcination at 773 K.

The crystallinity of the oxide support and the supported nanoparticles were determined by X-ray diffraction. The XRD powder patterns of CeO_2, Pt(N)/CeO_2 and Pt(Cl)/CeO_2 catalysts are reported in Fig. 1. For all samples it was possible to observe the six main characteristic peaks of the cubic phase, fluorite structure, of CeO_2, which are assigned to the (111), (200), (220), (311), (222) and (400) diffraction planes [20-23]. No diffraction peaks for platinum could be identified for both catalysts, consistent with the low platinum content or, more probably, a high Pt dispersion [8,20,24,25]. The crystal size for the ceria support, estimated by Scherrer's equation, was 17 nm.

TEM images for the samples (not shown) were consistent with XRD measurements. CeO_2 exhibited a high crystallinity with a plane distance of about 0.28 nm. The ceria particle size could not be calculated from the TEM images due to the high crystal agglomeration which makes difficult the determination of particle size distribution. Furthermore, the platinum particle size could not be quantified due to the high Pt dispersion (some small nanoparticles could be detected), in close agreement with XRD results. However, the presence of platinum nanoparticles was confirmed by EDS analysis. A similar observation was described in the literature for gold catalysts [26,27]. Small gold particles supported on ceria could not be detected by TEM due to the small contrast between the metal particle and the support.

The reducibility of the different catalysts was studied by temperature-programmed reduction under hydrogen. H_2-TPR profiles of CeO_2, Pt(N)/CeO_2 and Pt(Cl)/CeO_2 are shown in Fig. 2. The profile corresponding to the CeO_2 support exhibites reduction peaks at 760 and 1050 K, which can be attributed to surface and bulk reduction processes, respectively [25,28,29]. Pt addition to the CeO_2 support produced important changes in the TPR profiles. It is well known that cerium oxide reduction involves several processes: (i) the removal of surface carbonates [29], (ii) a change in the cerium oxidation state (Ce(IV) to Ce(III)) and (iii) -OH group formation by spillover of atomic hydrogen from Pt [28,29]. Furthermore, the surface reduction of ceria was shifted to lower temperatures in the presence of Pt [25]. This phenomenon can

be explained by the ability of the noble metal to dissociate hydrogen, thus promoting ceria reduction through spillover of hydrogen from the metal to the support [30].

Interestingly, both catalysts exhibited a reduction peak at low temperatures. However, the shape of this contribution was slightly different in the presence and absence of chlorine. For the chlorine-free catalyst, the hydrogen consumption peak (777.3 μmol $H_2.g^{-1}$) showed a main contribution at 610 K together with a shoulder at low temperatures (575 K). These two contributions include the surface reduction of ceria in close contact with the noble metal together with reduction of Pt species [22]. On the contrary, the chlorinated catalyst exhibited a single reduction peak centered at 590 K (652.6 μmol $H_2.g^{-1}$), which can be assigned to the reduction of surface ceria in close contact with platinum, as well as the breakdown of Pt-O-CeO_2 entities formed during the calcination treatment [22]. As shown in Table 1, the catalyst prepared with the chlorinated platinum precursor after calcination still contains a large amount of chlorine which could affect the reducibility of the support and, similarly, the oxygen mobility. Similar TPR profiles were previously reported for PtZn/CeO_2 catalysts prepared using two different Pt precursors (with and without chlorine) [22]. For the chlorine-free catalyst a broad hydrogen consumption peak was observed at low temperatures, which could be deconvoluted into two contributions. These two contributions were explained by the presence of a high degree of surface heterogeneity. Furthermore, in the case of the chlorinated catalyst, a delay in the metal reduction was observed due to the formation of CeOCl entities, which inhibited the metal-support interactions [22].

DRIFTS studies (discussed below) demonstrated that the chlorine-free catalyst exhibited a higher propensity for carbonate formation compared to the chlorinated catalyst. Consequently, the presence of an additional peak in the chlorine-free catalyst can also be associated to the involvement of these surface carbonate species in the reduction process at low temperature. Most probably, the reduction of carbonate to formate takes place at lower temperatures in the presence of Pt, through hydrogen spill-over phenomena. In this sense, it would be expected that this phenomena is inhibited in the presence of chlorine, due to formation of CeOCl species.

For the pre-treatment of these catalysts before the reaction, two reduction temperatures of 523 and 773 K were selected based on information obtained by TPR. These temperatures were selected in order to analyze the effect of the reduction treatment at low temperature, where only surface reduction processes are expected, compared to the high temperature reduction treatment, where additional reduction

processes, i.e. oxygen vacancy formation, are were expected. It is well known that, in the case of the chlorinated catalyst, an increase in the reduction temperature favors the formation of CeOCl entities, thus stabilizing Ce (III) species [17,31] and, consequently, producing a decrease of the OSC [22,29,32-34] . This effect could affect the catalytic activity and in fact, as will be discussed below, a poorer CO conversion in the case of the Cl-containing catalyst reduced at 773 K than reduced at 523 K was observed, probably due to decrease of the OSC. However, the opposite behavior has been found for the Cl-free catalyst.

The surface composition of the catalysts and the oxidation state of cerium were determined by XPS. Fig. 3(a) and (b) show the Ce 3d XPS spectra obtained with catalysts Pt(N)/CeO_2 and Pt(Cl)/CeO_2, respectively, both fresh and after *in situ* reduction at 523 and 773 K.

The spectra for the Ce 3d level have been studied by different authors, and their interpretation is not straightforward [22,29,32-34]. The two sets of spin-orbital multiplets, corresponding to the $3d_{3/2}$ and $3d_{5/2}$ contributions, are labeled *u* and *v*, respectively, and up to four peaks for each contribution can be obtained by a curve fitting analysis. Peaks labeled v_0 (880.8 eV), *v´*(885.6 eV), u_0 (898.6 eV), *u´*(904.7 eV), correspond to Ce (III) and peaks labeled *v* (882.5 eV), *v´´*(889.1 eV), *v´´´*(897.9 eV), *u* (901.1 eV), *u´´*(907.5 eV) and *u´´´*(916.8 eV), correspond to Ce (IV). The peaks labeled *v* and *v´´* have been assigned to a mixing of Ce $3d^9$ $4f^2$ O $2p^4$ and Ce $3d^9$ $4f^1$ O $2p^5$ Ce (IV) final states, and the peak denoted *v´´´* corresponds to the Ce $3d^9$ $4f^0$ O $2p^6$ Ce (IV) final state. On the other hand, lines v_0 and *v´* are assigned to the Ce $3d^9$ $4f^2$ O $2p^5$ and the Ce $3d^9$ $4f^1$ O $2p^6$ of Ce (III). The same assignation can be applied to the *u* structures, which corresponds to the Ce $3d_{3/2}$ levels.

XP spectra allow determination of the percentage of Ce (III) present in the catalyst surface and the oxidation state of the different metal species as a function of the reduction temperature. The degree of ceria reduction from XP spectra can be determined by the ratio between the sum of the intensities of bands corresponding to Ce (III) and the sum of the intensities of bands which correspond to Ce (III) and Ce (IV), following equation [32-34].

$$\%\ \text{Ce (III)} = 100 \cdot (I(v_0) + I(v') + I(u_0) + I(u')) / \sum(I(v^t) + I(u^t)) \qquad \text{Eq. 1}$$

The values obtained for the two catalysts after the different reduction treatments are reported in Table 2. Interestingly, there is a certain amount of Ce (III) already in the fresh (calcined) catalysts, around 37.0% of Ce (III). The presence of Ce (III) in the calcined catalyst has been attributed to the high energy of the X-ray beam which can produce a partial reduction of Ce (IV) ions during the XPS analysis [22,33,35]. In this sense XPS experiments were performed at low temperature (77 K) and the results showed that, in fact, a lower amount of Ce (III) was obtained under these conditions, *i.e.* 25.0% Ce (III) for the chlorine-free catalyst. On the other hand, it is well known that one of the parameters that affect the photo-reduction of CeO_2 during the XPS analysis is its crystallinity, in such a way that amorphous cerium oxide is reduced more extensively than crystalline cerium oxide [36]. However, taking into account that the same support was used for the preparation of the two Pt/CeO_2 catalysts, and that the XPS analysis was performed under the same experimental conditions, it can then be assumed that Ce (IV) photo-reduction due to the X-ray beam should be similar for both catalysts, and that any differences between them should be attributed to their distinctive chemical composition. Data in Table 2 show that the extent of Ce (IV) reduction increased after a reduction treatment at 523 K. The percentage of Ce (III) in these samples was close to 46.8 and 47.6 %, for the chlorine-free and the chlorinated catalyst, respectively. With the increase of the reduction temperature (up to 773 K) it was possible to observe a slight increase in the amount of Ce (III), and this rise is more pronounce for the Cl-containing catalyst. These results are were in agreement with previous data from our group [22], where a higher amount of Ce (III) in the $Pt(Cl)/CeO_2$ catalyst after a high temperature reduction treatment was detected. This fact was tentatively attributed to the presence of chlorine and, more specifically, to the formation of CeOCl species. Le Normand *et al*. [37] described the formation of the oxychloride species on a $Pd(Cl)/CeO_2$ catalyst after a reduction treatment at 673 K. According to these authors, no definitive changes were observed by XRD and XPS analysis, and the only evidence of a structural modification was the Cl/Ce molar ratio close to one, but just for low ceria content. In this context, Table 2 reports the Cl/Ce ratios for the $Pt(Cl)/CeO_2$ catalyst in the fresh and reduced states. Taking into account the Cl/Ce ratio after the reduction at 773 K, the value of 0.14 is quite different from the value of 1 reported in the literature [37]. However, due to the low chlorine content (because of the low platinum loading) in this catalyst, it would be reasonable to expect the formation of CeOCl microphases on just a small fraction of the ceria surface.

At this point it is worth noting that the presence of carbonates and -OH surface groups can be detected by XPS with a shift of the C 1s at about 288.5 eV [38] when the reduction temperature was increased, and this fact it was more pronounced in the case of chlorine-free catalyst. This result is in agreement with the DRIFTS spectra (see later), and provides some information about the reaction mechanism as observed below.

The XP spectra of the Pt 4f level in the Pt(N)/CeO_2 and Pt(Cl)/CeO_2 catalysts, both fresh (calcined) and *in situ* reduced at 523 and 773 K, are shown in Fig. 4 (a) and (b), respectively. The overall spectrum of the Pt 4f band appears as the sum of two broad bands corresponding to levels $4f_{7/2}$ (at lower binding energies) and $4f_{5/2}$ (at higher binding energies). The Pt $4f_{7/2}$ band was deconvoluted in two components, corresponding to Pt (II) (around 72.7 eV) and Pt (0) (around 70.4 eV) species. In the case of the Pt(N)/CeO_2 catalyst (Fig. 4 (a)), it was possible to observe that the fresh (calcined) sample presented a band centered at a binding energy of 72.4 eV corresponding to Pt (II) in different environments. After reduction at 523 K the peak broadens, and it could be deconvoluted into two contributions, centered at 72.4 and 71.4 eV, corresponding to Pt (II) and Pt (0), respectively. Finally, after the reduction treatment at 773 K, all platinum was in the metallic state. On the other hand, somewhat different behavior was observed for the Cl-containing catalyst (Fig. 4 (b)). In the fresh (calcined) sample, platinum was present as Pt (II) species, most likely originating during a reductive process taking place upon impregnation of the Pt (IV) precursor and the ceria support, and the subsequent calcination. After reduction at 523 K, some degree of Pt (II) reduction to metallic platinum has taken place, but to a lower extent than in the case of the non-chlorinated catalyst. Interestingly, complete reduction is not achieved even after reduction at 773 K, although, in this case, the amount of remaining Pt (II) species is very low.

In order to characterize the oxygen mobility in the Pt/CeO_2 catalysts, both in the presence of chlorine and in the Cl-free sample, an indirect method of determination was carried out using the temperature-programmed oxidation of previously adsorbed CO. The amount of CO desorbed, together with the amount of CO_2 formed upon oxidation with oxygen from the CeO_2 support, was monitored by on-line mass spectrometry. The CO_2 and CO desorption profiles obtained during the TPD analysis on catalysts reduced at 523 K are shown in Fig. 5 (a) and (b), respectively. As can be observed, the CeO_2 support did not adsorb CO and, consequently, CO_2 was not produced in the temperature range studied. This observation demonstrates the importance of the Pt nanoparticles to

chemisorb and oxidize CO to CO_2. Several authors have used CO-TPD for the characterization of CeO_2-based catalysts [39-42]. In the case of gold catalysts, two CO_2 desorption peaks were reported; the first one, around 433 K, is assigned to the oxidation of adsorbed species over noble metal nanoparticles, and the second one, near 773 K, is attributed to the decomposition of carbonate species on the support [43]. In the present work, the incorporation of Pt nanoparticles in the catalyst surface rise to a CO_2 desorption peak at around 380 K with a shoulder at about 425 K for both catalysts, irrespective of the presence or absence of chlorine (Fig. 5 (a)), although it was much more intense for the Cl-free catalyst. Ribeiro et al. [43] have proposed two mechanisms to justify the presence of these CO_2 desorption peaks. First, a CO disproportionation reaction on the Pt surface giving rise to CO_2 and $C_{(s)}$ as products. Carbon deposition is a well-known deactivation mechanism, which causes the loss of metal-support interactions and leads to the covering of the catalytic surface, which in turn hinders reactant adsorption on active sites. Secondly, these authors proposed that CO_2 could be formed by the oxidation of CO adsorbed on metal-support centers with oxygen coming from the support, forming CO_2 and leaving an oxygen vacancy. Previous studies described in the literature for Au/TiO_2 catalysts have suggested the adsorption of CO on gold nanoparticles and the reaction with lattice oxygen as the proposed mechanism for CO_2 formation at low temperatures [44]. Moreover, in the case of Au/ZrO_2 catalysts, two CO_2 desorption peaks were observed; the first one at 393 K and the second at 573 K. The first peak was due to CO disproportionation, but the second peak was related to the decomposition of carbonate species on the support surface[45]. Isotopic studies on Rh/CeO_2 catalysts carried out by Putna *et al*. [40] demonstrated that oxygen atoms resulting from CO dissociation quickly exchange with oxygen from the ceria lattice.

As observed in Fig. 5, the amount of CO desorbed is 10 times lower that the amount of CO_2 produced, indicating that in both cases, nearly all the CO adsorbed was oxidized to CO_2. However, a close inspection to the CO_2 desorption profiles (Fig. 5 (a)) shows that the amount of CO_2 formed was larger in the Cl-free catalyst. In addition to the main peak at 380 K, there is a high temperature shoulder for both catalysts, this contribution being more evident in the chlorine-free catalyst. The low temperature peak (main contribution) should be ascribed to CO oxidation on the Pt nanoparticles, whereas the high temperature shoulder can be attributed to carbonate decomposition. The larger amount of CO_2 formed in the absence of chlorine (976.3 μmol $CO_2 \cdot g^{-1}_{catalyst}$ *versus* 273.3 μmol $CO_2 \cdot g^{-1}_{catalyst}$), demonstrates that the presence of chlorine inhibited the

formation of carbonates, while the presence of CeOCl species prevented oxygen mobility, in agreement with the results showed previously.

The CO desorption profiles for both catalysts were very similar, Fig. 5 (b), with the amount of CO desorbed being 0.042 and 0.034 mmol $CO.g^{-1}_{catalyst}$ for the chlorine-free and the chlorinated catalyst, respectively. The presence of a wide desorption peak indicates indicated a heterogeneity of adsorption sites with different energies for CO desorption, which suggests the presence of a broad Pt particle size distribution [46]. Two peaks can be differentiated in the CO desorption profiles, one at low temperatures (380-390 K) and another one at high temperatures (420-440 K) [39]. CO desorption at low temperature is associated with linear CO adsorption over small Pt particles, while desorption at high temperature can be attributed to bridge bonded CO species, or CO species adsorbed in low coordinated surface sites where higher temperatures are required for desorption [46] and/or to the decomposition of carbonates. In this work, the $Pt(N)/CeO_2$ catalyst exhibited a slightly wider CO desorption profile compared to the $Pt(Cl)/CeO_2$ catalyst, thus suggesting a larger heterogeneity in the metal particle size distribution in the former. This observation will be confirmed later by infrared experiments.

Moreover, with the CO-TPD results it was possible to estimate the metal dispersion on the surface. Considering an adsorption stoichiometry of 1:1, platinum dispersions of 82 and 66% for the chlorine-free and chlorinated catalyst, respectively, were obtained.

3.2. Catalytic behavior.

3.2.1. CO PROX: effect of reaction and reduction temperature.

The reaction profiles in terms of CO conversion and yield to CO_2 for the CeO_2 support and the two catalysts, $Pt(N)/CeO_2$ and $Pt(Cl)/CeO_2$, at different reaction and reduction temperatures, are shown in Fig. 6 and Fig. 7, respectively (gas mixture feed: 2% CO, 2% O_2, 20% H_2 balanced in He, $\lambda = 2$).

The light-off curves in Fig. 6 show the influence of the reduction temperature in the CO conversion for the different catalysts. It was observed that both catalysts exhibited an important difference in the CO conversion with an increase in the reaction temperature. In the case of the chlorine-free catalyst, there is a gradual increase in CO conversion with temperature. On the contrary, the chlorinated catalyst exhibited a sharp

increase in the CO conversion at 353 K, reaching a final conversion value similar to its counterpart. This behavior may be associated to a different reaction mechanisms taking place on each of these catalysts. Details regarding the possible mechanisms are reported later. Both catalysts exhibited a decrease in CO conversion and selectivity to CO_2 (not shown) at temperatures above 400 K. At these high temperatures, the oxidation of H_2 to H_2O was more favored than the oxidation of CO to CO_2 [11,24,25,47]. However, the effect of CO_2 present in the reaction feed cannot be ruled out as being responsible for the loss in catalytic activity. Mariño et al. [11] proposed the formation of carbonates due to CO_2 adsorption on the ceria support as responsible for the observed behavior in the catalytic activity.

Concerning the effect of the Pt nanoparticles, it can be observed that the support alone is practically inactive over the range of temperatures studied, independent of the reduction temperature used. This observation is in close agreement with previous analyses [20,23]. Concerning the Pt-based catalysts, important changes in the catalytic activity were observed as a function of reduction temperature and precursor used. There was an increase in the catalytic activity in the temperature range between 320 and 380 K for both catalysts, up to a conversion value close to 90%. A closer inspection of these data shows that the chlorine-free catalyst presented a higher activity compared to the chlorinated catalyst, at least at low temperatures (333 K). The effect of the metal precursor was more pronounced after a reduction treatment at high temperature. Similar behavior was observed by Ko et al. [48] for Pd-Co/YSZ catalysts. In this sense, whereas an increase in the reduction temperature to 773 K was beneficial for the reaction process over Pt(N)/CeO_2 catalyst, i.e. there is a slight improvement in the catalytic activity at low temperature, the same variation in the reduction temperature is detrimental for the Pt(Cl)/CeO_2 catalyst. In accordance with the XPS results, an increase in the reduction temperature must give rise to an increase in the amount of oxygen vacancies created by reduction of Ce (IV) to Ce (III). Apparently, those oxygen vacancies at the metal-support interface favor the activation of the CO molecule and provide active sites for the oxidation to CO_2 [49]. On the contrary, in the chlorinated catalyst, chlorine inhibited the formation of those oxygen vacancies due to the formation of CeOCl surface species [22,50,51]. This process was favored at high reduction temperatures.

Complete O_2 conversion (not shown) was reached at 413 K for both catalysts reduced at 523 K. However, in the case of reduction at 773 K, complete O_2 conversion was observed at 433 K for the chlorine-free catalyst whereas it shifted to 413 K for the

chlorinated catalyst. The yield to CO_2 in the range of high CO conversion (~ 380-400 K) was around 0.4 for both catalysts (Fig. 7).

3.2.2. CO PROX: isothermal experiments.

To better illustrate the effect of the reaction temperature and to understand the differences in catalytic activity for the different catalysts, two experiments were carried out isothermally at 333 and 353 K with the Cl-containing and Cl-free catalysts, both reduced at 523 K (gas mixture feed 2% CO, 2% O_2, 20% H_2 balanced in He, $\lambda = 2$).

The same trend with regards to CO conversion was observed in the isothermal experiments (Fig. 8), and comparable to the behavior described in Fig. 6. At low temperature (333 K), the chlorinated catalyst exhibited poor catalytic activity (conversion around 2%), which remained constant with time on stream. On the contrary, and in accordance with data in Fig. 6, the Cl-free catalyst exhibited high catalytic activity (up to 73% conversion) which was accompanied by significant deactivation during the first minutes of the reaction, dropping to a steady state activity of around 12% conversion. The high catalytic activity, together with the large deactivation rate observed in the Cl-free catalyst clearly indicates the presence of a different reaction mechanism in the absence of chlorine at low temperatures. Most probably, this reaction mechanism involves surface species which are consumed during the first stages of the reaction. A completely different scenario occurred at a slightly higher reaction temperature (353 K). At this temperature, both catalysts exhibited a high catalytic activity (around 75-85% conversion), which remains more or less stable with time on stream.

The mechanism for the CO oxidation over reducible metal oxides catalyst was proposed by Mars and Van Krevelen [10,24,41,52,53]. In this mechanism CO is adsorbed on the surface of the noble metal and is activated by labile oxygen coming from the support. CO and H_2 compete for the same adsorption site but, at low temperature, CO adsorption is favored. The high catalytic activity observed at low temperature on the $Pt(N)/CeO_2$ catalyst compared to its chlorinated counterpart clearly reflects a different mechanism depending on the presence or absence of chlorinated species, most probably associated with the support. Ayastuy *et al.* [24] observed a similar divergence in the catalytic activity of Pt catalysts supported on Al_2O_3 and CeO_2. In this study, the catalytic activity of the Pt/CeO_2 catalyst was larger than that of the Pt/Al_2O_3 catalyst, these differences being associated with the different reaction

mechanisms taking place on the different catalysts. In the case of Al_2O_3, the CO oxidation reaction took place through the competitive Langmuir-Hinshelwood mechanism, where oxygen and CO compete with hydrogen for the active sites. In the case of CeO_2, the reaction mechanism was the non-competitive Mars-Van Krevelen, in which there is an important role for the oxide support. In the present work, the high CO conversion for the chlorine-free catalyst at low temperature must be attributed to the availability of active sites/species in the oxide support, which were blocked or absent when chlorine was present. Furthermore, the irreversible consumption of these surface species (more probably –OH species) favoring the catalytic process at low temperature would explain the fast deactivation observed in the initial steps of the reaction. A description of the different hypothesis to explain this behavior will be discussed in the subsequent section.

3.2.3. CO PROX: effect of feed composition.

Another factor that can influence the reaction mechanism when working with oxide supports is the feed composition, i.e. the λ value ($\lambda = 2(O_2)/(CO)$). The λ value was modified in this study by increasing the O_2 content in the reaction feed (2% CO, 0.6-2% O_2, 20% H_2 balanced in He). The evolution of the CO and O_2 conversion profiles together with the CO_2 selectivity for the $Pt(N)/CeO_2$ catalyst reduced at 523 K, and at a reaction temperature of 353 K, are reported in Fig. 9.

The CO conversion depends strongly on the λ value. Using an oxygen content above the stoichiometric value ($\lambda = 2$), i.e. when there is an excess of oxygen, both the CO and H_2 oxidation reactions are favored. However, the effect of this excess oxygen is more pronounced for the hydrogen oxidation reaction, i.e. there is in general a decrease in the selectivity to CO_2 with increasing oxygen content. It must be kept in mind that ceria can act as an oxygen buffer. As a result, the oxygen concentration over the catalyst would be virtually constant up to a certain oxygen inlet concentration, when the maximum oxygen storage capacity (OSC) of ceria is exceeded [11]. This result is in agreement with the values reported in the literature [10,13,24,36,53] which show a similar dependence of the CO oxidation reaction with the λ value. Mariño et al. [10] studied the influence of the gas composition for platinum and iridium catalysts. For both systems, the CO and H_2 oxidation rates were increased with an increase in the λ value, while the selectivity towards CO_2 formation fell.

3.2.4. CO PROX monitored by operando DRIFT spectroscopy: effect of the reaction temperature.

In order to analyze the different steps taking place during the course of the catalytic reaction, both Pt/CeO_2 catalysts have been analyzed by *operando* DRIFTS. The spectra obtained for CO oxidation are shown in the Fig. 10 (a), (b) and (c) for CeO_2, $Pt(N)/CeO_2$ and $Pt(Cl)/CeO_2$, respectively.

DRIFTS experiments showed the presence of formate and carbonates species as identified by bands between 1570 and 1200 cm^{-1}, in accordance with earlier observations [13,41,50,54-56]. Interestingly, carbonate and formate bands were very similar (in magnitude) on the CeO_2 support and on the $Pt(Cl)/CeO_2$ catalyst, whereas they were much more intense for in the Cl-free catalyst, in agreement with the CO_2-TPD results, shown in Fig. 5. The Cl-free catalyst showed bands at 1567, 1547, 1462, 1369 and 1292 cm^{-1}, attributed to the presence of different modes of carbonate species, and formate. On the contrary, the chlorinated catalyst showed bands at 1462 and 1362 cm^{-1}, corresponding to polydentate carbonate [13,41,53,55,56]. The presence of formate was confirmed by peaks at 2926 cm^{-1} and 2840 cm^{-1}, which are characteristic of –CH stretching vibrations, these bands being more pronounced for the Cl-free catalyst. These observations suggest that the presence of chlorine hinders the formation of surface formates. Furthermore, both catalysts showed the presence of bands in the region between 3500 and 3000 cm^{-1}, assigned to surface hydroxyl groups (-OH) and residual water molecules adsorbed on the support.

During the course of the PROX reaction, an increase in the reaction temperature for the Cl-free catalyst gave rise to a decrease in the signals attributed to water and hydroxyls groups (bands at 3640, 3511, and ~ 3180 cm^{-1}), this decrease being acute in the temperature range 313-333 K. Furthermore, an increase in reaction temperature produced a significant decrease in the intensity of the carbonate bands at 1567 and 1292 cm^{-1}. For the chlorinated catalyst, only a slight decrease in the bands due to surface –OH groups or carbonates was observed. The differences between the DRIFT spectra for both catalysts may be related with the differences observed in catalytic activity. As described in the literature [13,56,57], the surface -OH groups may facilitate the formation of carbonate species by reaction with CO. Föttinger *et al.* [56] suggested that the formation of carbonates may be associated with two models, the first one being related with the dissociation of CO on the noble metal followed by the reaction of CO_2 with the support to form the surface carbonates, and the second one being related with

the direct reaction between CO and -OH groups of the support, followed by CO_2 reaction with additional -OH groups. As described above, at 333 K, the Cl-free catalyst presented a higher catalytic activity and a large deactivation rate with time on stream (Fig. 9). Initially, CO can react with -OH surface groups of the support to form carbonates and formates until total saturation; then, the reaction could move towards Pt surface sites, leading to a lesser, but constant activity. Shido *et al.* [58] studied Rh/CeO_2 in the WGS reaction and observed the formation of bidentate formates from CO and surface -OH groups on ceria. Daté *et al.* [15] studied the influence of humidity on the CO oxidation reaction on gold catalysts prepared on different supports. According to these authors, the reaction mechanism depends on the nature of the support and on the presence of moisture; moisture improves the reaction activity due to the involvement of -OH group as intermediates. Xu *et al.* [59] also studied the reaction mechanism of WGS and PROX reactions. In this case, CO_2 formation occurred through the reaction between adsorbed CO and surface -OH groups (CO_{ads} + OH_{surf}) taking place at Pt-oxide interface sites at low temperature. Graf *et al.* [60] determined that the reactivity of hydroxyl groups on Pt catalysts for the WGS reaction is associated with the formate formation by mono-coordinated hydroxyls.

The existence of CO species adsorbed on the support and on the Pt nanoparticles can be followed by bands in the range 2240-1860 cm^{-1} [61]. Peaks at 2172 and 2116 cm^{-1} are due to gas phase CO although they may cover contributions due to CO adsorbed on Ce (IV) and Ce (III) sites, respectively. Peaks at 2070 and 2052 cm^{-1} in the case of Cl-containing catalyst and at 2032 cm^{-1}, in the case of Cl-free catalyst, are assigned to CO species adsorbed on Pt. The presence of this band at lower wavenumbers in the Cl-free catalyst could be associated with the presence of small nanoparticles together with the presence of defect sites, i.e. oxygen vacancies, at the metal-support interface which are able to tilt CO adsorption [61]. On the contrary, the peak at 2070 cm^{-1} in the chlorinated catalyst can indicate the presence of metal atoms in less dense close packed terraces, e.g. (100) faces, whereas the peak at ~ 2052 cm^{-1} could be associated with the presence of Pt atoms in defect sites (in steps and corners). The presence of the band at 2032 cm^{-1} may suggest the presence of defect sites which were able to activate the CO molecule on the Cl-free catalyst, these sites being likely candidates to promote the CO oxidation reaction. Badri *et al.* [50] also observed a similar shift in the CO band induced by chlorine species. In agreement with these results, this shift was due to the formation of an active electronegative species by chlorine. The characteristic bands for gas phase

CO was observed in the range 2120-2170 cm^{-1} [13,55]. In this region, bands corresponding to CO adsorbed on sites belonging to a CeOCl phase, where Ce (IV) was reduced to Ce (III), can be found. They appear at around 2175 cm^{-1} [50]; therefore, they could be difficult to identify due to overlap.

Furthermore, and in agreement with the TPD based CO desorption profile, it is interesting to mention that the Pt(N)/CeO_2 catalyst presented a wider Pt-CO desorption profile than the Cl-free catalyst, this indicating the higher surface heterogeneity for the former catalyst.

The changes observed in the surface chemistry of the Cl-free catalyst by DRIFT after an increase in the reaction temperature from 313 to 333 K (Fig. 10), fit with the results obtained in the light-off curves for the PROX reaction (Fig. 8), (in both cases the catalysts were reduced at 523 K). These observations suggest that the high activity obtained at low temperature (333 K) by the Cl-free catalyst must be attributed to the participation of the support in the reaction process. Apparently, the Pt(N)/CeO_2 catalyst presented surface hydroxyl species capable of participating in the reaction process at low temperature as follows:

$$CO_{ads} + 2\ OH_{surf} \rightarrow CO_2 + H_2O$$

Moreover, some authors [62-64] suggest that the PROX reaction generates a -HCOO intermediate by reaction between CO and -OH groups. This hypothesis can be confirmed by performing reaction studies at constant temperature during several hours (Fig. 8). Whereas the chlorinated catalyst showed almost no activity, the Cl-free catalyst showed an initially high activity (CO conversion about 75%), together with a high degree of deactivation (down to a 13% conversion) after 2 h reaction at 333 K. On the contrary, the PROX reaction performed at a higher temperature (353 K) proceeded with high conversion for both catalysts (~ 80%), which remained constant with reaction time. Therefore, these observations clearly demonstrate that the high catalytic activity of Pt(N)/CeO_2 at low temperature (333 K) compared with the chlorinated catalyst, can be attributed to the presence of reactive -OH species on the surface of the support, which reacts to generate CO_2 and H_2O. The presence of a finite number of surface -OH groups on the catalyst could justify the limited activity of this catalyst at 333 K compared to the same behavior at 353 K. In this respect, a shift in the reaction mechanism is expected at 353 K to the surface of the platinum nanoparticles, for both catalysts, without the

involvement of surface -OH species from the support, i.e., reaction between adsorbed CO and oxygen from the metal-support interface sites.

4. Conclusions.

Two catalysts prepared using different platinum precursors (with and without chlorine) were assessed in the preferential CO oxidation reaction in the presence of H_2. From the obtained results it was possible to conclude that the Cl-free catalyst showed better activity at low temperature (333 K) than the chlorinated catalyst. At temperatures above 373 K, the CO oxidation reaction occurred *via* the same mechanism on both catalysts (interfacial reaction centers between CO adsorbed on Pt and oxygen from the support). However, at low temperatures, the presence of a second reaction mechanism in the Cl-free catalyst was involved. This mechanism seems to involve the participation of -OH groups from the support, with the corresponding consumption of CO and subsequent formation of CO_2. It has been possible to confirm this hypothesis by (i) DRIFTS studies under reaction conditions, in which a drastic drop in the hydroxyl signal after an increase in reaction temperature from 313 to 333 K was observed and, (ii) reaction studies at constant temperature, which showed a rapid deactivation along with the formation of CO_2, due to the limited amount of available -OH surface groups to reacted with CO.

Acknowledgments

The authors gratefully acknowledge financial support from Ministerio de Ciencia e Innovación (Spain) (Project MAT2010-21147) and the Generalitat Valenciana (PROMETEO/2009/002 – FEDER and PROMETEOII/2014/004). EOJ thanks the CNPq – Brazil for her grant. We thank S.B. Campbell and F.M. McKenna (University of Aberdeen) for assistance in performing the DRIFT experiments.

References

[1]. A. Demirbas, Biohydrogen: For Future Engine Fuel Demands (Springer-Verlag London Limited, London, 2009).

[2]. G.W. Huber, S. Iborra, A. Corma, Chem. Rev. 106 (2006) 4044-4098.

[3]. J.I.L. Hurtado, B.Y.M. Soria, El Hidrógeno y la Energía (Asociación Nacional de Ingenieros del ICAI, Madrid, 2007).

[4]. K. Liu, C. Song, V. Subramani (Eds), Hydrogen and Syngas Production and Purification Technologies (Wiley, Canada, 2009).

[5]. J.A. Turner, Science 285 (1999) 687-689.

[6]. R. Farrauto, S. Hwang, L. Shore, W. Ruettinger, J. Lampert, T. Giroux, Y. Liu, O. Ilinich, Annu. Rev. Mater. Res. 33 (2003) 1-27.

[7]. R.M. Navarro, M.A. Peña, J.L.G. Fierro, Chem. Rev. 107 (2007) 3952-3991.

[8]. E. Simsek, S. Özkara, A.E. Aksoylu, Z.I. Önsan, Appl. Catal. A: Gen. 316 (2007) 169-174.

[9]. J.M. Zalc, D.G. Löffler, J. Power Sources 111 (2002) 58-64.

[10]. F. Mariño, C. Descorme, D. Duprez, Appl. Catal. B: Envir. 54 (2004) 59-66.

[11]. F. Mariño, C. Descorme, D. Duprez, Appl. Catal. B: Envir. 58 (2005) 175-183.

[12]. W. Li, F.J. Gracia, E.E. Wolf, Catal. Today 81 (2003) 437-447.

[13]. O. Pozdnyakova, D. Teschner, A. Wootsch, J. Kröhnert, B. Steinhauer, H. Sauer, L. Toth, F.C. Jentoft, A. Knop-Gericke, Z. Paál, R. Schlögl, J. Catal. 237 (2006) 1-16.

[14]. E. Quinet, L. Piccolo, F. Morfin, P. Avenier, F. Diehl, V. Caps, J.L. Rousset, J. Catal. 268 (2009) 384-389.

[15]. M. Daté, M. Okumura, S. Tsubota, M. Haruta, Angew. Chem. Int. Ed. 43 (2004) 2129-2132.

[16]. M.A. Debeila, R.P.K. Wells, J.A. Anderson, J. Catal. 239 (2006) 162-172.

[17]. L. Kepinsk, J. Okal, J. Catal. 192 (2000) 48-53.

[18]. D. Briggs, M.P. Seah, Practical Surface Analysis (Wiley, Chichester, 1992).

[19]. A. Sepúlveda-Escribano, F. Coloma, F. Rodríguez-Reinoso, J. Catal. 178 (1998) 649-657.

[20]. I. Dobrosz-Gómez, I. Kocemba, J.M. Rynkowski, Appl. Catal. B: Envir. 83 (2008) 240-255.

[21]. H.S. Roh, H.S. Potdar, K.W. Jun, S. Han, J.W. Kim, Catal. Lett. 93 (2004) 203-207.

[22]. J. Silvestre-Albero, F. Coloma, A. Sepúlveda-Escribano, F. Rodríguez-Reinoso, Appl. Catal. A: Gen. 304 (2006) 159-167.

[23]. M. Thammachart, V. Meeyoo, T. Risksomboon, S. Osuwan, Catal. Today 68 (2001) 53-61.

[24]. J.L. Ayastuy, A. Gil-Rodríguez, M.P. González-Marcos, M.A. Gutiérrez-Ortiz, Int. J. Hydrogen Energy 31 (2006) 2231-2242.

[25]. J.L. Ayastuy, M.P. González-Marcos, A. Gil-Rodríguez, J.R. González-Velasco, M.A. Gutiérrez-Ortiz, Catal. Today 116 (2006) 391-399.

[26]. G. Avgouropoulos, M. Manzoli, F. Boccuzzi, T. Tabakova, J. Papavasiliou, T. Ioannides, V. Idakiev, J. Catal. 256 (2008) 237-247.

[27]. H. Sakurai, T. Akita, S. Tsubota, M. Kiuchi, M. Haruta, Appl. Catal. A: Gen. 291 (2005) 179-187.

[28]. P. Fornasiero, G. Balducci, R. Di Monte, J. Kaspar, V. Sergo, G. Gubitosa, A. Ferrero, M. Graziani, J. Catal. 164 (1996) 173-183.

[29]. S. Ricote, G. Jacobs, M. Milling, Y. Ji, P.M. Patterson, B.H. Davis, Appl Catal. A: Gen. 303 (2006) 35-47.

[30]. J.C. Serrano-Ruiz, G.W. Huber, M.A. Sánchez-Castillo, J.A. Dumesic, F. Rodríguez-Reinoso, A. Sepúlveda-Escribano, J. Catal. 241 (2006) 378-388.

[31]. F. Fajardie, o. Tempere, J.M. Manoli, G. Djega-Mariadassou, G. Blanchard, J. Chem. Soc. , Faraday Trans. 94 (1998) 3727-3735.

[32]. R. Leppelt, B. Schumacher, V. Plzak, M. Kinne, R.J. Behm, J. Catal. 244 (2006) 137-152.

[33]. J. Silvestre-Albero, F. Rodríguez-Reinoso, A. Sepúlveda-Escribano, J. Catal. 210 (2002) 127-136.

[34]. F. Zhang, P. Wang, J. Koberstein, S. Khalid, S.W. Chan, Surf. Sci. 563 (2004) 74-82.

[35]. P.O. Larsson, A. Andersson, J. Catal. 179 (1998) 72-89.

[36]. M.S. Francisco, V.R. Mastelaro, P.A.P. Nascente, A.O. Florentino, J. Phys. Chem. B 105 (2001) 10515-10522.

[37]. F. Le Normand, L. Hilaire, K. Kili, G. Krill, G. Maire, J. Phys. Chem. 92 (1988) 2561-2568.

[38]. A. Pulido, P. Concepcion, M. Boronat, C. Botas, P. Alvarez, R. Menendez, A. Corma, J. Mater. Chem. 22 (2012) 51-56.

[39]. R.K. Herz, D.F. McCready, J. Catal. 81 (1983) 358-368.

[40]. E.S. Putna, R.J. Gorte, J.M. Vohs, G.W. Graham, J. Catal. 178 (1998) 598-603.

[41]. D. Teschner, A. Wootsch, O. Pozdnyakova-Tellinger, J. Kröhnert, E.M. Vass, M. Hävecker, S. Zafeiratos, P. Schnörch, P.C. Jentoft, A. Knop-Gericke, R. Schlögl, J. Catal. 249 (2007) 318-327.

[42]. P. Thormählen, M. Skoglundh, E. Fridell, B. Andersson, J. Catal. 188 (1999) 300-310.

[43]. N.F.P. Ribeiro, F.M.T. Mendes, C.A.C. Perez, M.M.V.M. Souza, M. Schmal, Appl. Catal. A: Gen. 347 (2008) 62-71.

[44]. M. Haruta, S. Tsubota, T. Kobayashi, H. Kageyama, M.J. Genet, B. Delmon, J. Catal. 144 (1993) 175-192.

[45]. P. Konova, A. Naydenov, C. Venkov, D. Mehandjiev, D. Andreeva, T. Tabakova, J. Molecular Catal. A: Chem. 213 (2004) 235-240.

[46]. R. Padilla, M. Benito, L. Rodríguez, A. Serrano-Lotina, L. Daza, J. Power Sources 192 (2009) 114-119.

[47]. Z. Lendzion-Bielun, M.M. Bettahar, S. Monteverdi, D. Moszynski, U. Narkiewicz, Catal. Lett. 134 (2010) 196-203.

[48]. E.Y. Ko, E.D. Park, H.C. Lee, D. Lee, S. Kim, Angew. Chem. Int. Ed. 46 (2007) 734-737.

[49]. P. Concepción, A. Corma, J. Silvestre-Albero, V. Franco, J.Y. Chane-Ching, J. Am. Chem. Soc. 126 (2004) 5523-5532.

[50]. A. Badri, C. Binet, J.C. Lavalley, J. Phys. Chem. 100 (1996) 8363-8368.

[51]. A. Wootsch, C. Descorme, D. Duprez, J. Catal. 225 (2004) 259-266.

[52]. A. Hornés, A.B. Hungría, P. Bera, A.L. Cámara, M. Fernández-Garcáa, A. Martínez-Arias, L. Barrio, M. Estrella, G. Zhou, J.J. Fonseca, J.C. Hanson, J.A. Rodríguez, J. Am. Chem. Soc. 132 (2009) 34-35.

[53]. A. Martínez-Arias, A.B. Hungría, M. Fernández-García, J.C. Conesa, G. Munuera, J. Power Sources 151 (2005) 32-42.

[54]. P. Bera, A. Hornés, A.L. Cámara, A. Martínez-Arias, Catal. Today 155 (2010) 184-191.

[55]. C. Binet, M. Daturi, J.C. Lavalley, Catal. Today 50 (1999) 207-225.

[56]. K. Föttinger, R. Schlogl, G. Rupprechter, Chem. Commun. 2008) 320-322.

[57]. H. Tanaka, M. Kuriyama, Y. Ishida, S.i. Ito, T. Kubota, T. Miyao, S. Naito, K. Tomishige, K. Kunimori, Appl. Catal. A: Gen. 343 (2008) 125-133.

[58]. T. Shido, Y. Iwasawa, J. Catal. 141 (1993) 71-81.

[59]. L. Xu, Y. Ma, Y. Zhang, Z. Jiang, W. Huang, J. Am. Chem. Soc. 131 (2009) 16366-16367.

[60]. P.O. Graf, D.J.M. de Vlieger, B.L. Mojet, L. Lefferts, J. Catal. 262 (2009) 181-187.

[61]. F. Coloma, J. Coronado, C. Rochester, J. Anderson, Catal. Lett. 51 (1998) 155-162.

[62]. A.B. Mhadeshwar, D.G. Vlachos, J. Phys. Chem. B 108 (2004) 15246-15258.

[63]. K-i. Tanaka, M. Shou, H. He, X. Shi, X. Zhang, J. Phys. Chem. C 113 (2009) 12427-12433.

[64]. K-i. Tanaka, M. Shou, Y. Yuan, J. Phys. Chem. C 114 (2010) 16917-16923.

5: Figure

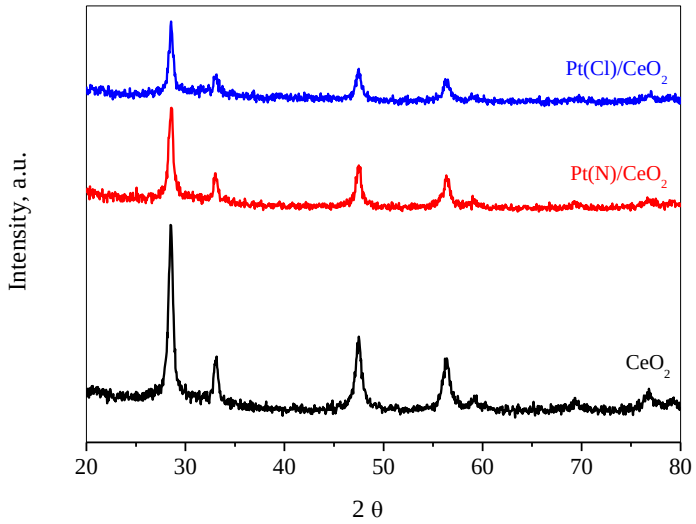

Fig. 1. Powder XRD patterns of CeO_2, Pt(N)/CeO_2 and Pt(Cl)/CeO_2.

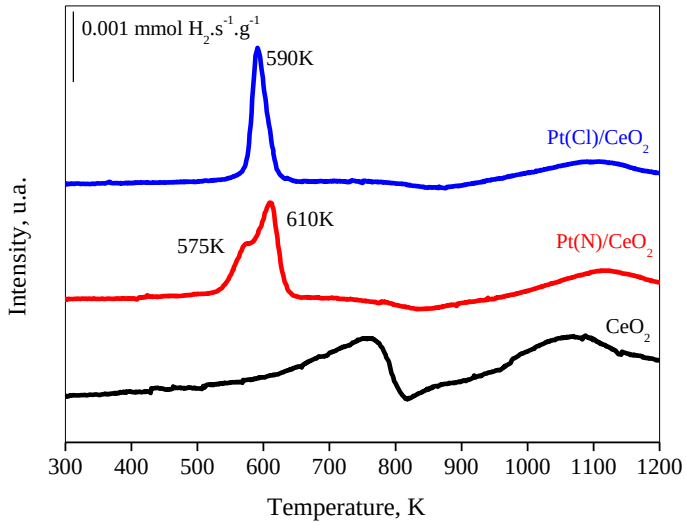

Fig. 2. TPR profiles of CeO_2, Pt(N)/CeO_2 and Pt(Cl)/CeO_2.

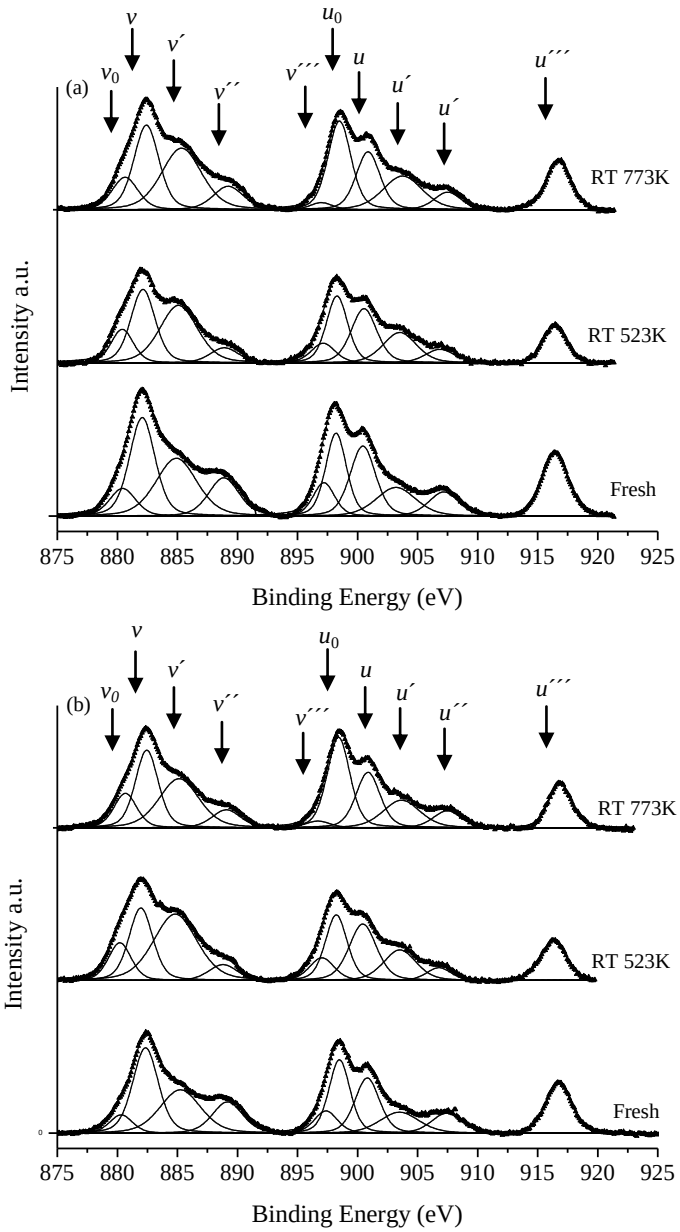

Fig. 3. XPS Ce 3d spectra of the fresh and reduced at 523 and 773 K Pt(N)/CeO_2(a) and Pt(Cl)/CeO_2 (b) catalysts.

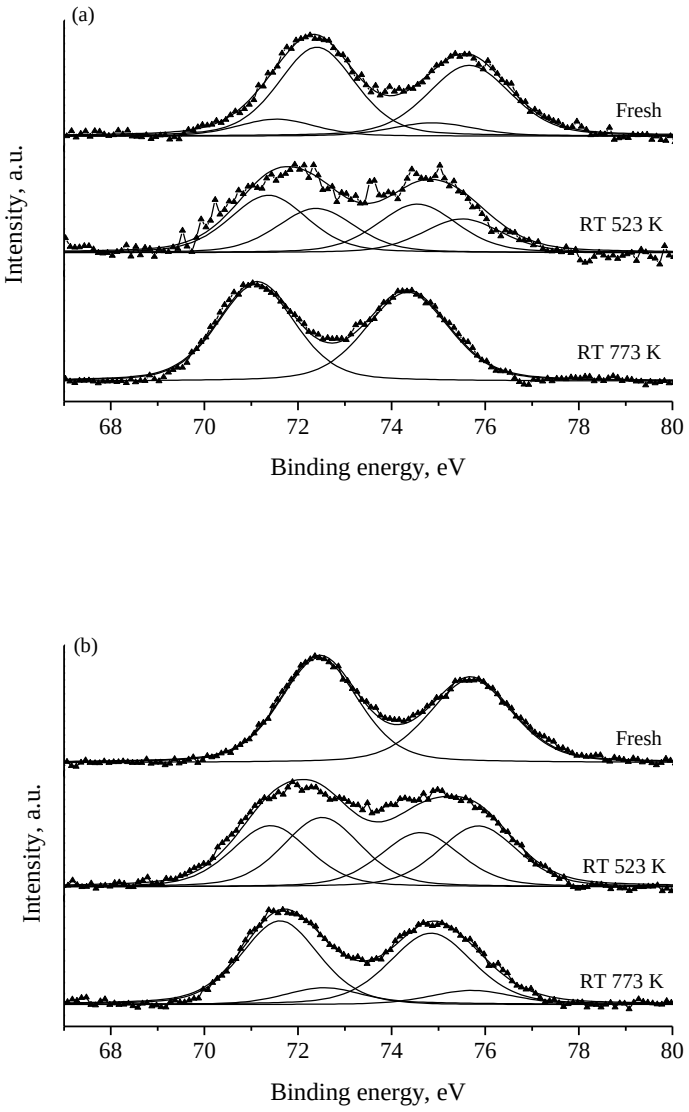

Fig. 4. XP spectra of the Pt 4f level of Pt(N)/CeO_2 (a) and Pt(Cl)/CeO_2 (b) catalysts, fresh and reduced *in situ* at 523 K and 773 K.

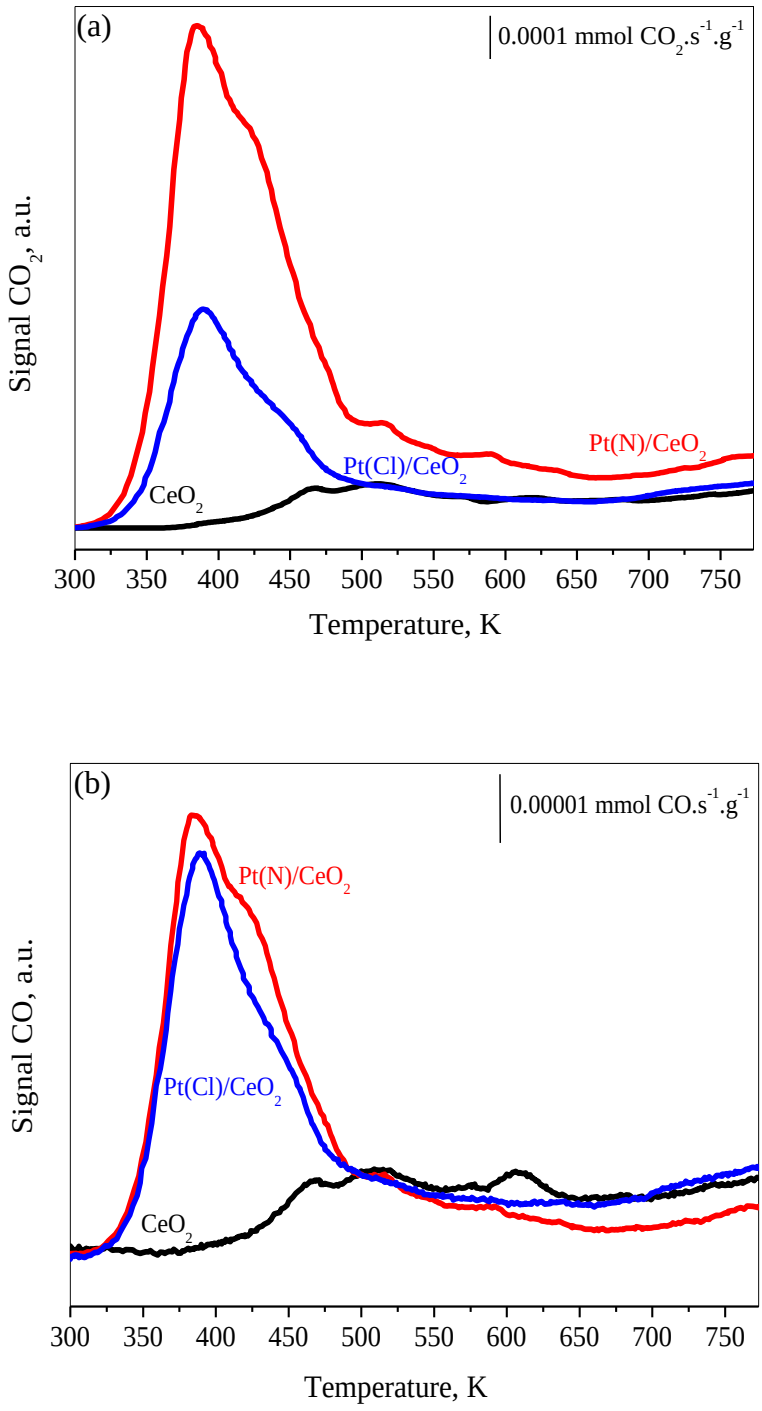

Fig. 5. Desorption profiles of (a) CO_2 and (b) CO from CeO_2, $Pt(N)/CeO_2$ and $Pt(Cl)/CeO_2$ catalysts, reduced at 523 K.

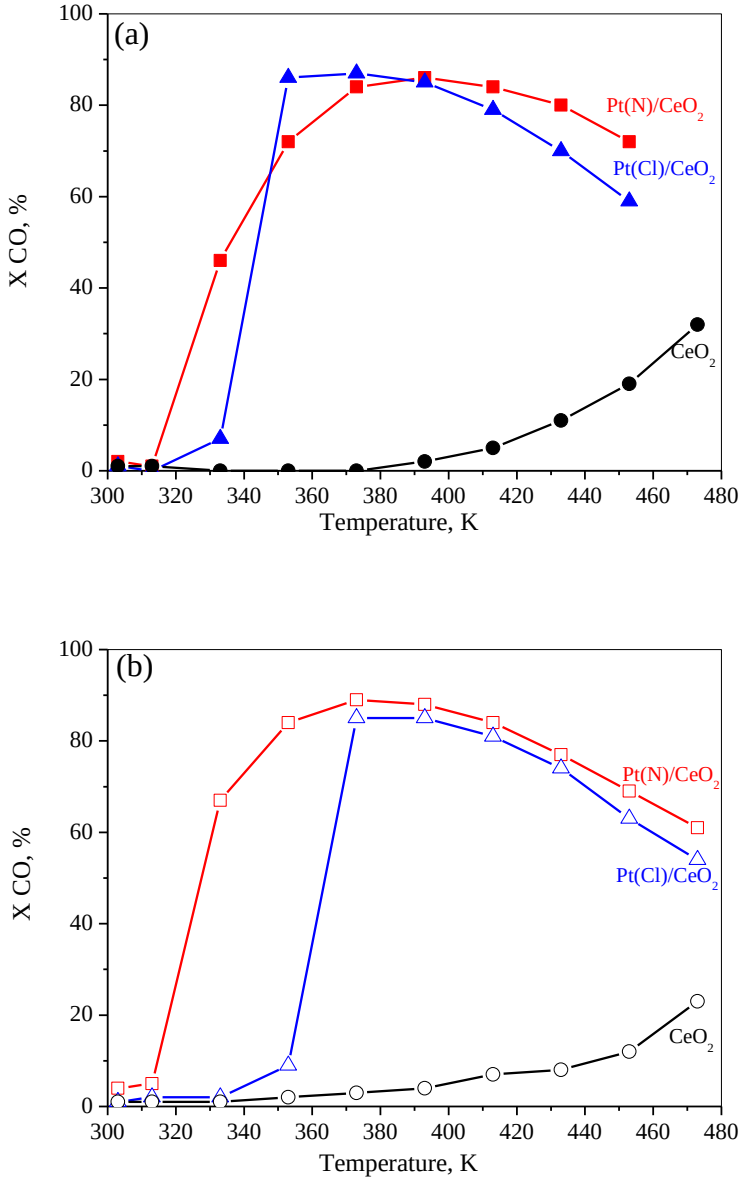

Fig. 6. CO oxidation light-off curves for CeO_2, Pt(N)/CeO_2 and Pt(Cl)/CeO_2 catalysts, reduced at 523 K (a) and at 773 K (b).

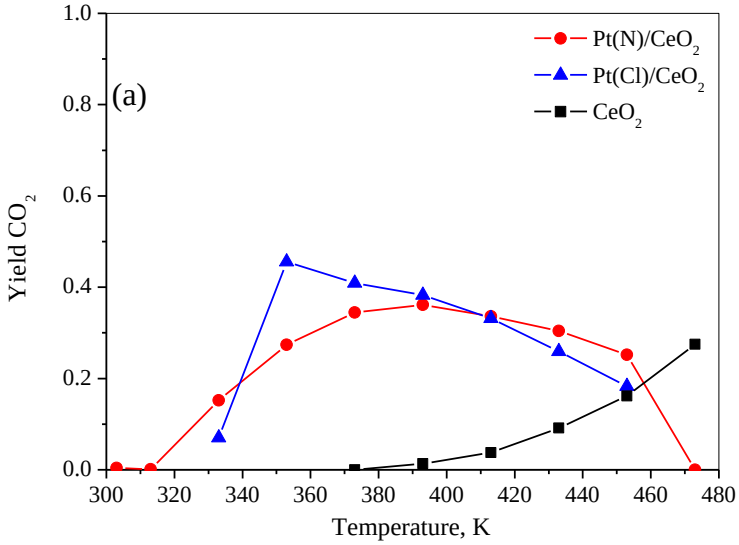

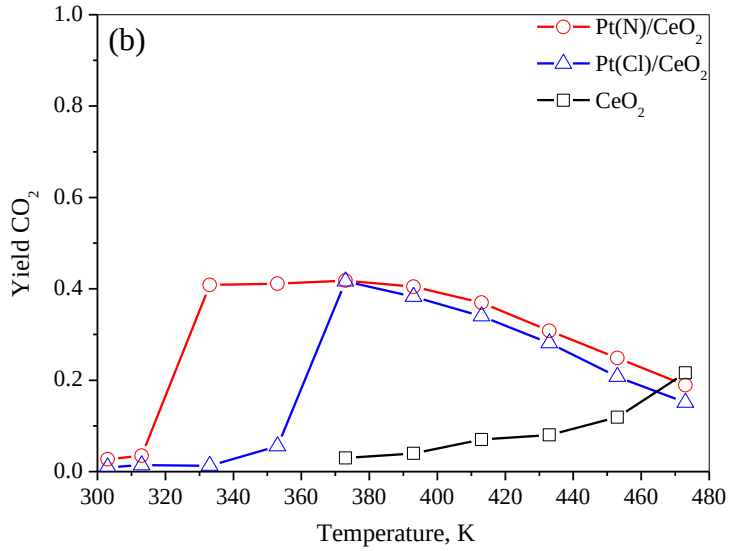

Fig. 7. CO_2 yield profiles for CeO_2, Pt(N)/CeO_2 and Pt(Cl)/CeO_2 catalysts, reduced at 523 K (a) and at 773 K (b).

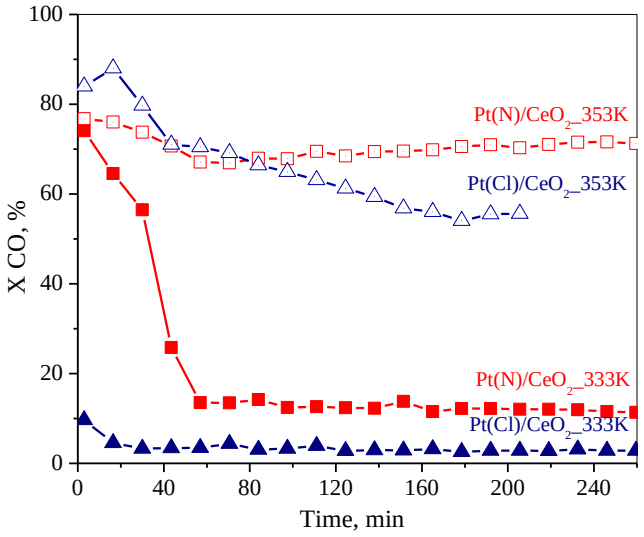

Fig. 8. CO conversion at 333 K (closed symbols) and 353 K (open symbols) for $Pt(N)/CeO_2$ and $Pt(Cl)/CeO_2$ catalysts reduced at 523 K.

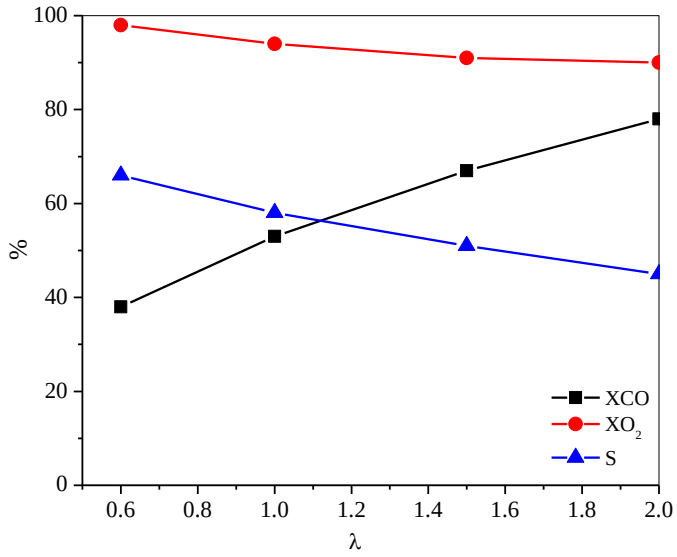

Fig. 9. CO preferential oxidation as a function of λ at 353 K on Pt(N)/CeO_2 catalyst, reduced at 523 K, in a feed of 2% CO, 0.6-2% O_2, 20% H_2 and balance He.

(a)

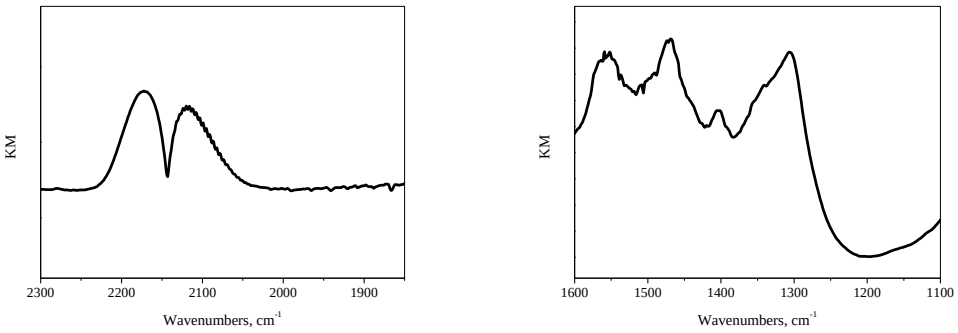
KM
2300
2200
2100
2000
1900
Wavenumbers, cm-1
KM
1600
1500
1400
1300
1200
1100
Wavenumbers, cm-1

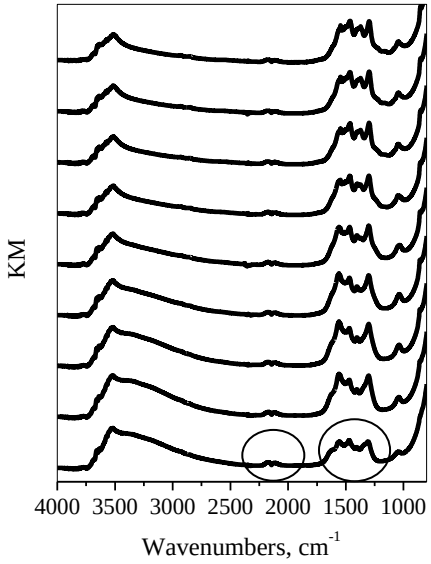
KM
4000 3500 3000 2500 2000 1500 1000
Wavenumbers, cm-1

(b)

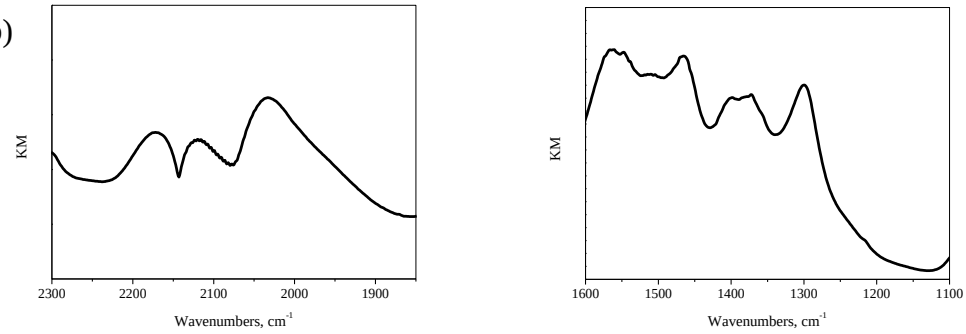
KM
2300
2200
2100
2000
1900
Wavenumbers, cm-1
KM
1600
1500
1400
1300
1200
1100
Wavenumbers, cm-1

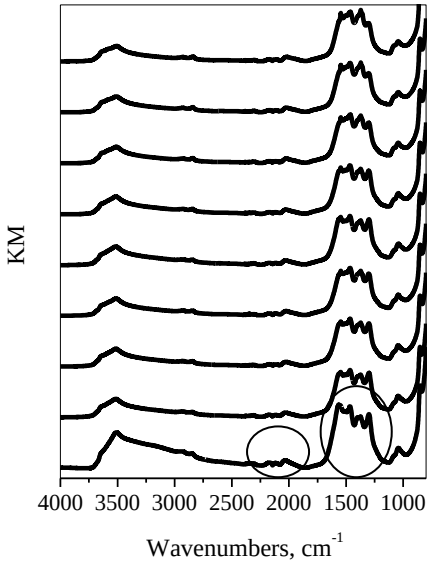
KM
4000 3500 3000 2500 2000 1500 1000
Wavenumbers, cm-1

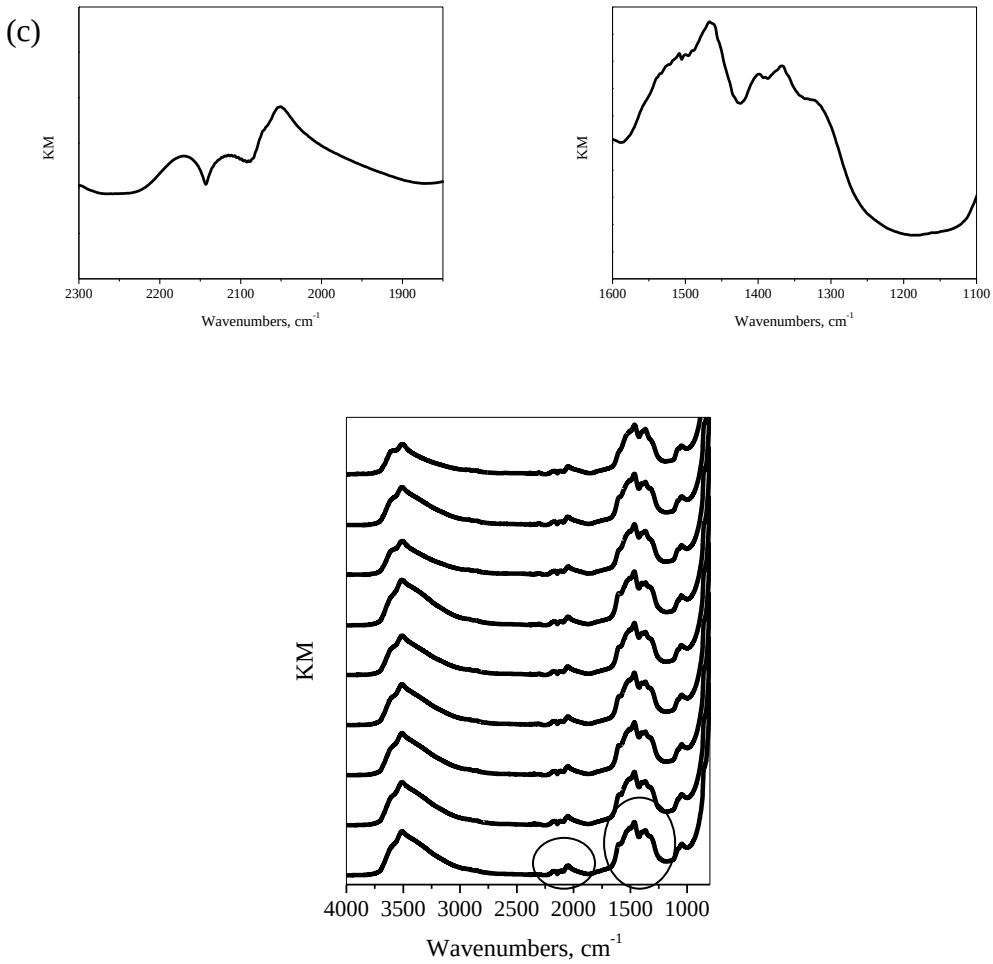

Fig. 10. DRIFT spectra of CO oxidation under 2% CO, 10% air, 20% H_2 and balance N_2 feed for CeO_2 (a), Pt(N)/CeO_2 (b) and Pt(Cl)/CeO_2 (c). Initial temperature was 313 K and increased in 20 K increments from bottom to top.

6: Table

Table 1. BET surface area and Pt and Cl content.

Catalysts	S_{BET}, $m^2.g^{-1}$	Pt, %	% Cl
CeO_2	110	---	---
Pt(N)/CeO_2	75	1.0	---
Pt(Cl)/CeO_2	95	1.0	0.7

Table 2. XPS characterization of Pt(N)/CeO_2 and Pt(Cl)/CeO_2 catalysts.

Catalyst	Red. Temp./K	% Ce(III)	Cl/Ce
Pt(N)/CeO_2	Fresh	37.5	---
	523	46.8	---
	773	47.4	---
Pt(Cl)/CeO_2	Fresh	37	0.13
	523	47.6	0.15
	773	47.9	0.14